

KAN-AD: Time Series Anomaly Detection with Kolmogorov–Arnold Networks

Quan Zhou^{*}, Changhua Pei, Haiming Zhang,
Gaogang Xie, Jianhui Li[†]
Computer Network Information Center
Chinese Academy of Science
zhouquan,chpei,hai,xie,lijh@cnic.cn

Jing Han, Zhengwei Gao
ZTE
China
han.jing28,gao.zhengwei@zte.com.cn

Fei Sun
Institution of Computing Technology
Chinese Academy of Science
sunfei@ict.ac.cn

Dan Pei
Computer Science Department
Tsinghua University
peidan@tsinghua.edu.cn

Abstract

Time series anomaly detection (TSAD) has become an essential component of large-scale cloud services and web systems because it can promptly identify anomalies, providing early warnings to prevent greater losses. Deep learning-based forecasting methods have become very popular in TSAD due to their powerful learning capabilities. However, accurate predictions don't necessarily lead to better anomaly detection. Due to the common occurrence of noise, i.e., local peaks and drops in time series, existing black-box learning methods can easily learn these unintended patterns, significantly affecting anomaly detection performance. Kolmogorov–Arnold Networks (KAN) offers a potential solution by decomposing complex temporal sequences into a combination of multiple univariate functions, making the training process more controllable. However, KAN optimizes univariate functions using spline functions, which are also susceptible to the influence of local anomalies. To address this issue, we present KAN-AD, which leverages the Fourier series to emphasize global temporal patterns, thereby mitigating the influence of local peaks and drops. KAN-AD improves both effectiveness and efficiency by transforming the existing black-box learning approach into learning the weights preceding univariate functions. Experimental results show that, compared to the current state-of-the-art, we achieved an accuracy increase of 15% while boosting inference speed by 55 times.

1 Introduction

Time Series Anomaly Detection (TSAD) has become an essential part of IT infrastructure [16, 24, 28, 30] and manufacturing [14, 38, 39, 48] because it can promptly identify potential anomalies, providing timely alerts or sufficient clues for fault localization. TSAD greatly enhances system reliability by identifying anomalies in key performance indicators, attracting significant research attention in recent years [10, 15, 18, 35].

Thanks to the powerful learning capabilities of neural networks and the proposal of self-supervised AD algorithms, TSAD based on deep learning [41, 45, 50] has gradually replaced rule-based methods [5, 33] and become the new state-of-the-art. These approaches aim to learn normal patterns from historical data, enabling the

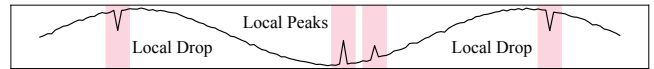


Figure 1: Illustration of local drops and peaks.

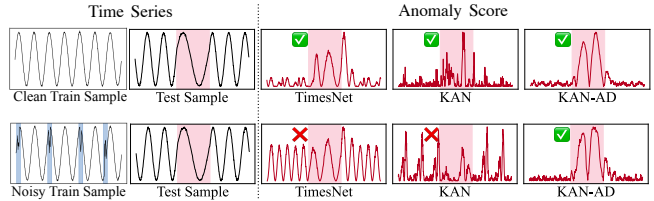


Figure 2: The black curve represents the original sample, with local peaks and dips highlighted in blue. The red curve denotes the anomaly scores provided by the method, the actual anomalous sections are highlighted in pink. The upper part demonstrates that when trained on the clean normal sample, all three methods successfully detect the anomaly segment. The lower part shows that when trained on data containing anomalies, TimesNet and KAN are disrupted by the anomalous samples, rendering them unable to detect anomaly segments.

identification of anomalies by comparing predicted values to actual observations. Anomalies are detected when deviations between the predicted and actual values exceed a certain threshold.

Although deep learning-based TSAD algorithms demonstrate excellent detection accuracy compared to rule-based methods, it is challenging to achieve further improvements in detection accuracy. Our investigation shows, as illustrated in Figure 1, that local peaks and drops are quite common in time series data. Some clustering-based methods, such as SubLOF [5], can partially resist the effects of such noisy data, but their overall detection accuracy is not sufficient. Many deep learning methods [37, 41], on the other hand, are easily affected and tend to learn these noises to some extent, making it difficult to effectively model the expected normal patterns. As a result, they struggle to accurately identify anomalies when compared to the actual occurring time series.

Kolmogorov–Arnold Networks (KANs) [26, 27] offers a potential solution to this challenge by revisiting the modeling of complex data. Based on the Kolmogorov–Arnold representation theorem [4, 20, 21], KANs decompose complex objectives into a combination

^{*}Also affiliated with University of Chinese Academy of Sciences.

[†]Corresponding author.

of multiple univariate functions which can be learned via neural networks using spline functions [7]. This design retains the learning capabilities of deep learning while allowing intervention in the learning process to prevent neural networks from being disturbed by local peaks or drops, making it particularly useful for TSAD.

KAN's decomposition of complex objectives has shown promise in achieving accurate representations [1, 47]. However, directly applying KAN to TSAD poses significant challenges. From the upper part of Figure 2, it can be observed that models trained on clean training samples, such as TimesNet [41] (third column) and KAN (fourth column), successfully detect anomalies in the test samples. This is manifested by the increasing anomaly scores of these two algorithms on the anomalous time series segments. When focusing on the bottom row of Figure 2, we find that even KAN fails to detect anomalies when the training samples contain noisy samples. The main reason is that, although KAN can specify univariate functions, these functions are not specifically designed for time series and can still overfit local features, failing to completely eliminate the impact of local peaks or drops.

To address these challenges, we propose KAN-AD, a KAN for special designed TSAD. By considering the characteristics of time series, we redesign KAN's univariate function set and adopt Fourier series, which represent periodic functions as sums of sine and cosine components. Since its components possess local smoothness, during the learning process, we freeze the functions during training and only learn their coefficients, reducing the impact of local peaks and drops while preserving strong learning capabilities. This approach effectively mitigates the impact of local peaks and drops while maintaining strong learning capabilities. Compared to spline functions adopted by KAN, Fourier series naturally extract frequency domain information from the time series, which can better model global pattern and effectively handle local fluctuations without being affected by them [8, 34].

Additionally, we enhance KAN-AD's ability to capture periodicity by designing a periodic univariate function. To eliminate the negative impact of trend components in TSAD, we design an extra bias univariate function together with differencing mechanism. Through KAN-AD, TSAD is no longer a black-box fitting the relationships between points in the time series. Instead, it efficiently learns the coefficients of specially designed univariate functions to model normal time series patterns. This design brings a dual enhancement in both efficiency and effectiveness to TSAD. Experimental results show that KAN-AD detects with an F1 accuracy that is 29% higher while being 36% faster than KAN.

Our contributions are as follows:

- We are the first to introduce the Kolmogorov-Arnold representation theorem into the TSAD field. By reformulating the problem, the detection accuracy is improved and the complexity of the model is significantly reduced.
- We propose KAN-AD, a novel TSAD method. By carefully designing univariate functions, KAN-AD not only achieves higher detection accuracy compared to KAN, but its inference speed is also faster.
- We conducted extensive experiments on four public datasets. Compared to the current state-of-the-art method, KAN-AD

achieves an accuracy increase of 15% while boosting inference speed by 55 times.

2 Preliminaries and Problem Formulation

2.1 Problem Statement

This paper primarily addresses the issue of anomaly detection in single time series curves, also known as univariate time series (UTS). To elaborate on the problem more comprehensively, consider the following UTS observational data: $x_{0:t} = \{x_0, x_1, x_2, \dots, x_t\}$ and anomaly labels $C = \{c_0, c_1, c_2, \dots, c_t\}$, where $x_t \in \mathbb{R}$, $c \in \{0, 1\}$, and $t \in \mathbb{N}$. Here, $x_{0:t}$ represents the entire observed time series, and C denotes the temporal anomaly labels.

Given a UTS $x = [x_0, x_1, x_2, \dots, x_t]$, the objective of UTS anomaly detection is to utilize the data $[x_0, x_1, \dots, x_i]$ preceding each point x_i to predict c_i .

2.2 Kolmogorov–Arnold Networks

Kolmogorov–Arnold Networks (KAN) [26, 27] is a novel neural network architecture that builds on the Kolmogorov–Arnold representation theorem [4, 20, 21]. This theory provides a theoretical basis for decomposing continuous multivariate functions into multiple univariate function combinations.

2.2.1 Theoretical Foundation. The Kolmogorov–Arnold representation theorem demonstrates that any multivariate continuous function can be decomposed into a finite sum of univariate functions, as shown in Equation (1), where $\varphi_{q,p}$ are univariate functions that map each input variable x_p , and Φ_q are continuous functions.

$$f(x_1, x_2, \dots, x_n) = \sum_{q=1}^{2n+1} \Phi_q \left(\sum_{p=1}^n \varphi_{q,p}(x_p) \right) \quad (1)$$

$$\text{KAN}(x) = (\Phi_{L-1} \circ \Phi_{L-2} \circ \dots \circ \Phi_0)(x) \quad (2)$$

2.2.2 Network Architecture. KAN consists of a series of interconnected univariate sub-networks, each responsible for learning distinct features of the data. Unlike traditional multi-layer perceptrons (MLPs), which employ fixed activation functions at each node, KAN replaces each weight parameter with a univariate function. The resulting functional form for deeper KAN can be expressed as Equation (2), where each Φ_l represents a layer of univariate functions applied to the input or intermediate outputs.

2.2.3 B-spline Functions. The vanilla KAN [26, 27] utilizes B-spline functions [7] to optimize the representation of univariate functions. While B-spline functions demonstrate strong performance in approximating localized characteristics, particularly for non-linear data with local variations, this capability may also lead to fitting anomalous features in the data. Since anomalies often present themselves as localized patterns [45], B-splines may inadvertently capture these outliers, potentially reducing the robustness of the model.

Table 1 lists commonly used polynomial functions for time series analysis. In KAN, the choice of univariate function has a significant impact on the model's performance. We further investigate the influence of different univariate functions on anomaly detection performance in Section 4.5.

Table 1: Commonly used univariate functions for time series approximation.

Name	$\Phi_n(x)$
Taylor Series	x^n
Fourier Series	$\cos(nx) + \sin(nx)$
Chebyshev Polynomial I	$\cos(n \arccos(x))$
Chebyshev Polynomial II	$\frac{\sin((n+1) \arccos(x))}{\sin(\arccos(x))}$

3 Methodology

The primary challenge in anomaly detection within real-world time series is the accurate identification of “normal” patterns by learning the pattern of historical time series containing anomalies [25]. The prevailing method of directly modeling the relationship between the future value x_{i+1} at time $i + 1$ and the historical data $x_{0:i}$ from time 0 to i is often affected by local peaks and drops in the data.

To address this challenge, we propose KAN-AD, which integrates the Fourier series [9] with the Kolmogorov-Arnold representation theorem. KAN-AD reframes the task of learning normal patterns as the estimation of coefficients for univariate functions. By leveraging the global representation provided by the Fourier series, KAN-AD effectively reduces the influence of local drops and peaks in historical data. As shown in Figure 3b, the pipeline of KAN-AD consists of three main stages: **mapping**, **reducing**, and **projection**. During the mapping and reducing phases, the input time window is processed through a univariate function and weighted by coefficients to generate a representation robust to local anomalies. Finally, in the projection stage, the prediction for x_{i+1} is made.

Specifically, in the mapping phase, we activate the univariate functions with the input time window $x_{0:i}$ for reconstructing normal pattern. In the reducing phase, the reconstruction is formulated as a weighted sum of multiple univariate functions, where the weights are automatically learned from historical data. Finally, in the projection phase, future time series values x_{i+1} are predicted based on the reconstructed normal time series $x'_{0:i}$. Once the future normal pattern of the input time series is predicted, it can be compared with future real-time happening time series to detect anomalies.

In the following part of this section, we first provide a high-level, mathematical explanation of the entire workflow and principles of KAN-AD. Subsequently, we delve into the specific implementations of the mapping, reducing and projection phases.

3.1 Design of KAN-AD

As shown in Figure 3a, compared with KAN, KAN-AD focuses on learning the coefficients of univariate functions on edges, rather than relying on spline functions to optimize univariate functions themselves. In our approach, the neural network Θ no longer directly learns the temporal dependencies between a time window and the subsequent point. Instead, it focuses on *capturing the relationship between the time window and the coefficients of univariate functions*.

Formally, for KAN-AD, we employ Fourier series for normal pattern representation. In this way, $f(x)$, the mapping function

between the historical window $x_{0:i}$ and its normal pattern $x'_{0:i}$, can be expanded as the combination of multiple univariate functions, which is shown in Equation (3).

We posit the normal pattern can be represented by the finite N terms of the series [4, 20, 21], denoted as $g(x)$. The terms beyond the N -th term encompass the remaining stochastic observational noise $\epsilon(x)$.

$$f(x) = A_0 + \underbrace{\sum_{n=1}^N A_n \cos(nx) + B_n \sin(nx)}_{g(x)} + \underbrace{\sum_{n=N+1}^{\infty} A_n \cos(nx) + B_n \sin(nx)}_{\epsilon(x)} \quad (3)$$

We call this decomposition the function deconstruction (FD) mechanism. Following the decomposition, we aim to learn the coefficients preceding the different univariate functions. The normal pattern x' can then be expressed as in Equation (4), where \mathbf{H} denotes the univariate function matrix.

$$\begin{aligned} \mathbf{H} &= \text{Stack}(\cos(x_{0:i}), \sin(x_{0:i}), \dots, \cos(nx_{0:i}), \sin(nx_{0:i})) \\ \Theta(x_{0:i}) &= [A_1, B_1, A_2, B_2, \dots, A_n, B_n] \\ x'_{0:i} &= A_0 + \Theta(x_{0:i}) \times \mathbf{H} \end{aligned} \quad (4)$$

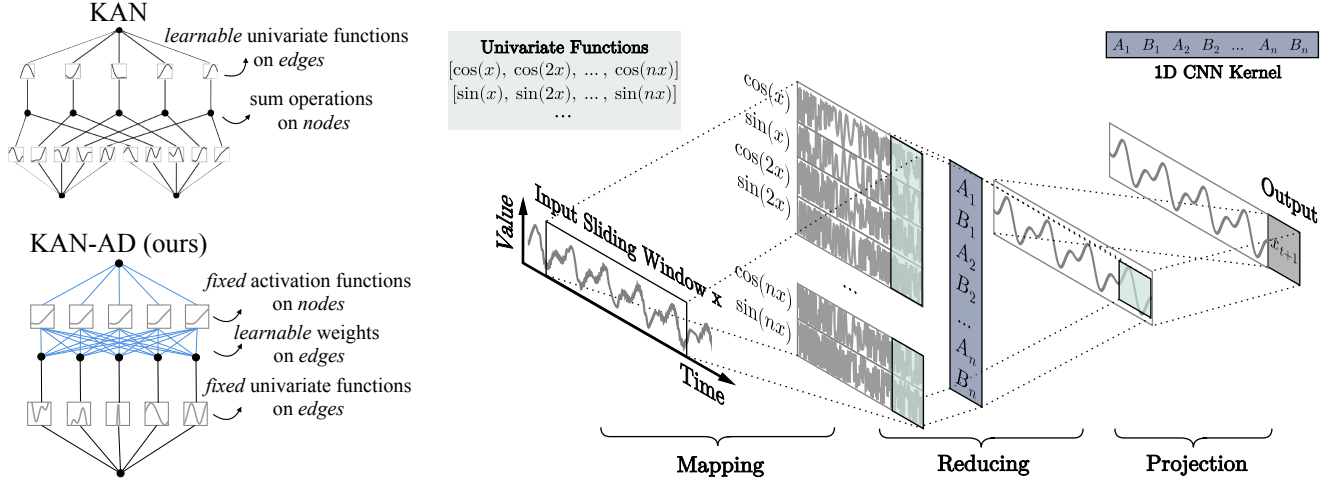
3.2 Mapping Phase

As shown in Figure 3b, the primary purpose of the mapping phase is to transform the original time series signal $x_{0:i} \in \mathbb{R}^T$ into multiple new sets of values $x_{0:i} \in \mathbb{R}^{T \times (N+N)}$ through a series of univariate functions. Here, T is the size of the sliding window. The first N represents the number of sine series univariate functions, and the other N represents the number of cosine series univariate functions. The detailed calculation method is shown in Equation (3).

Notably, besides the univariate function terms, an A_0 term representing the average value within the sliding window is also present, which varies across different windows. To mitigate the impact of fluctuating A_0 on coefficient fitting, a constant term elimination module is employed.

Constant Term Elimination: As shown in Equation 3, a constant term A_0 always exists during the approximation process. In Fourier series, A_0 represents the mean value of the function. Although normalization ensures that the entire time series has a mean of zero, individual time windows may still exhibit significant fluctuations in their means due to the presence of a trend. These variations in the constant term ultimately affect the model’s accurate estimation of Fourier coefficients, leading to biases in the construction of the normal pattern.

To mitigate the impact of mean fluctuations on the model’s approximation of normal time series patterns, we employ *first-order differencing* during data preprocessing to minimize the residual trend component in the data and subsequently renormalize the differenced data. This strategy allows the model to focus on estimating Fourier coefficients $A_{1:n}$ and $B_{1:n}$, thereby avoiding the need to learn frequently changing constant terms. After this differential



(a) Illustration of learning components in KAN and KAN-AD. KAN-AD learns the coefficients on edges with fixed univariate functions, and performs weighted sum operations on nodes. Blue lines indicate edges with weights.

(b) Illustration of the KAN-AD process using a sliding window approach. During the mapping phase, raw time windows are transformed into multiple univariate functions. In the reducing phase, a one-dimensional convolutional kernel learns coefficients for these univariate functions, aggregating them into a normal pattern for the current time window. In the projection phase, a single-layer MLP predicts future normal patterns.

Figure 3: Illustration of KAN-AD.

strategy, the normal pattern x' can be expressed as in Equation (5).

$$x'_{0:i} \sim \Theta(x_{0:i}) \times \mathbf{H} \quad (5)$$

$$f[i] = \frac{1}{T} \sum_{n=0}^{T-1} a_n \cos\left(\frac{2\pi ni}{T}\right) + b_n \sin\left(\frac{2\pi ni}{T}\right) \quad (6)$$

$$\mathbf{X} = x_{0:i}$$

$$S_n = \{\sin(nx_{0:i}), \cos(nx_{0:i})\}$$

$$P_n = \left\{ \sin\left(\frac{2\pi ni}{T}\right), \cos\left(\frac{2\pi ni}{T}\right) \right\} \quad (7)$$

Periodic-Enhanced KAN-AD: Time series often exhibit latent dependencies that are difficult to capture directly from the time domain but become evident in the frequency domain [32, 40]. Previous methods relied on Fast Fourier Transform (FFT) [3] to learn statistical features of different frequency components, neglecting the inherent approximation potential of sine and cosine functions used as univariate functions in the inverse FFT (iFFT). To enhance KAN-AD's ability to represent periodicity, we also incorporate frequency domain information. As shown in Equation (6), the iFFT process involves a weighted summation of sine and cosine components for each frequency component. This can be viewed as a special form of univariate function, namely a series containing $\cos(\frac{2\pi ni}{T})$ and $\sin(\frac{2\pi ni}{T})$, where i represents the index within the window. Consequently, it can be utilized for function approximation.

We integrate these functions as part of the univariate functions and, similar to the aforementioned approximation strategy, employ a one-dimensional convolutional network to learn the coefficients of these univariate functions. In our implementation, we ultimately employed the three univariate functions shown in Equation (7), namely the raw time variable X , the Fourier series S_n , and the

sine-cosine wave P_n . This strategy enables the combination of time-domain and frequency-domain univariate functions, thereby further improving KAN-AD's capability to capture normal patterns in time series.

3.3 Reducing Phase

Another major challenge in real-world time series anomaly detection is the high computational cost. Existing methods often overlook the increasing computational overhead when pursuing detection accuracy, making it impractical to deploy these algorithms in resource-constrained or large-scale settings.

Due to the function deconstruction (FD) mechanism, modeling normal pattern no longer requires fine-grained weight adjustments for every value within the entire time window. Instead, it only necessitates adjusting coefficients corresponding to the univariate functions. Since the number of univariate functions is significantly smaller than the length of the time window, the FD mechanism reduces the model's parameter count compared to modeling dependencies between each time point.

To fully leverage the advantages of the FD mechanism and accurately estimate univariate function coefficients, we employed a stacked one-dimensional convolutional neural network (1D CNN) to learn these coefficients. One-dimensional convolutions are well-suited for sequence modeling tasks due to their ability to traverse data along the temporal dimension. Moreover, the convolutional kernels in a 1D CNN can capture the diverse features introduced by the FD mechanism.

As show in Equation (8), KAN-AD first computes the required univariate functions for a given time window and combines them into a univariate function matrix $\mathbf{H}^{(0)}$.

$$\mathbf{H}^{(0)} = \text{Stack}(X, S_1, P_1, \dots, S_n, P_n) \forall n \in [1, 2, \dots, N] \quad (8)$$

The matrix is processed using multiple stacked one-dimensional convolutional layers with a kernel size of 3, allowing us to learn the coefficient matrix and progressively approximate the normal pattern, as illustrated in Equation (9). In Equation (11), each one-dimensional convolution with c channels applies a kernel W_c to each channel H_c . Here, the indices m and t denote positions within the convolutional kernel and the time window, respectively. We apply batch normalization [17] after each convolutional layer to ensure training stability and reduce internal covariate shift, as shown in Equation (10). Gaussian Error Linear Units (GELUs) [12] are utilized for activation:

$$\mathbf{H}^{(l)} = \text{CNN}(\text{CNN}(\mathbf{H}^{(l-1)})) \quad \forall l \in [1, 2, \dots, L] \quad (9)$$

where L denotes the number of 2-layer CNN blocks, and the network $\text{CNN}(\mathbf{H})$ and the convolution operation $\text{Conv}(\mathbf{H})$ are represented as:

$$\text{CNN}(\mathbf{H}) = \text{GELU}(\text{BN}(\text{Conv}(\mathbf{H}))) \quad (10)$$

$$\text{Conv}(\mathbf{H}) = \sum_{c=1}^{2N} \sum_{m=0}^2 W_c[m] \cdot \mathbf{H}_c[i+m-1] \quad (11)$$

At the final stage of the reducing phase, we employ a residual connection [11] between the hidden state $\mathbf{H}^{(L)}$ generated through L convolutional blocks and the original stacked input $\mathbf{H}^{(0)}$ to maintain the numerical stability of the univariate function matrix, as shown in Equation (12). Then, we use a convolutional kernel with a width of 1 to reduce the dimensional of the $\mathbf{H}^{(L)'}$ to generate the approximation of the normal mode within the current time window x' :

$$\mathbf{H}^{(L)'} = \mathbf{H}^{(L)} + \mathbf{H}^{(0)} \quad (12)$$

$$x'_{0:i} = \text{GELU}(\text{BN}(\text{DownConv}(\mathbf{H}^{(L)' }))) \quad (13)$$

Here, $\text{DownConv}(\mathbf{H}) = \sum_{c=1}^{2N} W_c \cdot \mathbf{H}_c[i]$ denotes the convolution operation for reducing dimensions.

3.4 Projection Phase

After obtaining an approximation x' of the current window’s normal mode, we predict the future normal mode x_{t+1} . Leveraging the accuracy of KAN-AD in approximating the normal mode, prediction becomes straightforward and can be achieved with a single-layer MLP:

$$x_{t+1} = W \cdot x'_{0:i} + b \quad (14)$$

where W denotes the weight matrix of the linear layer, and b represents its bias term.

4 Evaluation

In this section, we conduct comprehensive experiments primarily aimed at answering the following research questions.

RQ1: How does KAN-AD compare to state-of-the-art anomaly detection methods in performance and efficiency?

RQ2: How sensitive is KAN-AD to hyperparameters?

RQ3: How effective is each design choice in KAN-AD?

RQ4: How sensitive is KAN-AD to anomalies in the training data?

Table 2: Dataset Statistics.

Dataset	Curves	Train	Train Ano%	Test	Test Ano%
KPI	29	3,073,567	2.70%	3,073,556	1.85%
TODS	15	75,000	5.32%	75,000	6.38%
WSD	210	3,829,373	2.43%	3,829,537	0.76%
UCR	203	3,572,316	0.00%	7,782,539	0.47%

4.1 Experimental settings

This section details the datasets used for experimental comparison and outlines the experimental setup, including model training and dataset partitioning for the evaluation in this study.

4.1.1 Dataset. We evaluate the efficacy of the KAN-AD method for anomaly detection using four publicly available UTS datasets widely adopted in the field. These datasets span diverse domains and encompass a variety of anomaly characteristics, including KPI [6], TODS [22], WSD [49], and UCR [42].

Table 2 summarizes the characteristics of the datasets used, including the number of curves, dataset size, and anomaly rate. To further describe the distribution of anomaly interval lengths, we plot the cumulative distribution function (CDF) of interval lengths for each dataset in Figure 6. While most anomalies are relatively short, comprising less than 10 points, the WSD and UCR datasets exhibit a wide range of anomaly lengths, with the longest anomaly segments exceeding 300 points. This diversity in anomaly lengths allows for a more comprehensive evaluation of models’ anomaly detection capabilities.

For details regarding the provenance and characteristics of the datasets used, please refer to Appendix A.

4.1.2 Model training and inference. In our anomaly detection experiments, we trained a dedicated model for each time series within each dataset. These models were subsequently employed to generate detection outputs on their corresponding test sets. A batch size of 1024 was used by default, with a learning rate set to 0.01. Training for each time series was limited to a maximum of 100 epochs. To ensure model generalizability and mitigate overfitting, we incorporated validation sets into the training process. Specifically, for the UCR dataset, 20% of the training data was allocated as a validation set. For other datasets, we adopted a 4:1:5 ratio for splitting the data into training, validation, and test sets, respectively. During model testing, we set the batch size to 1 to facilitate a more accurate comparison of inference efficiency across different methods.

To enhance the reliability of our experimental results, we conducted five independent trials using different random seeds. The final results were reported as the mean and standard deviation across these trials, as presented in Table 3.

4.2 Baselines and metrics

This section details the SOTA methods employed for comparative analysis, followed by a description of the rigorous metrics used to evaluate detection accuracy. To ensure unbiased comparisons, we utilized publicly available source code implementations of the SOTA methods and excluded any post-processing operations, such as Point-adjust (PA), prior to submitting prediction results.

Table 3: Performance comparison. Best scores are highlighted in bold, and second best scores are highlighted in bold and underlined. Metrics include F1 (Best F1), $F1_e$ (Event F1), $F1_d$ (Delay F1), AUPRC (area under the precision-recall curve) and Avg $F1_e$ (average $F1_e$ score across four datasets).

Method	KPI				TODS				WSD				UCR				Avg $F1_e$
	F1	$F1_e$	$F1_d$	AUPRC	F1	$F1_e$	$F1_d$	AUPRC	F1	$F1_e$	$F1_d$	AUPRC	F1	$F1_e$	$F1_d$	AUPRC	
SRCNN	0.4137	0.0994	0.2266	0.3355	0.6239	0.1918	0.4399	0.6076	0.4092	0.1185	0.1951	0.3080	0.5964	0.1369	0.1656	0.5109	0.1367
SAND	0.2710	0.0397	0.1097	0.2022	0.5372	0.1879	0.5103	0.5145	0.1761	0.0839	0.1267	0.1238	0.7044	<u>0.5108</u>	<u>0.5116</u>	0.6550	0.2056
AT	0.6103	0.3020	0.3623	0.5676	0.4875	0.1915	0.2918	0.4148	0.4348	0.2311	0.1517	0.3527	0.6135	0.1696	0.1084	0.5458	0.2236
TranAD	0.7553	0.5611	0.6399	0.7399	0.5035	0.2460	0.3619	0.4501	0.7570	0.6338	0.4158	0.7106	0.5278	0.1840	0.1554	0.4599	0.4062
SubLOF	0.7273	0.2805	0.4994	0.7015	0.7997	0.4795	0.7169	0.7809	0.8683	0.6585	0.4917	0.8353	<u>0.8468</u>	0.4772	0.4151	<u>0.8001</u>	0.4739
TimesNet	0.8022	0.6363	0.6995	0.8166	0.6232	0.3327	0.4495	0.6031	0.9406	0.8444	0.6170	0.9376	0.5273	0.1805	0.1439	0.4536	0.4985
FITS	0.9083	0.6353	0.8175	0.9359	0.7773	0.5416	0.6312	0.7725	0.9732	0.8391	0.6535	0.9771	0.6664	0.2926	0.2912	0.5969	0.5772
OFA	0.8810	0.6150	0.7952	0.9009	0.6928	0.5811	0.5588	0.7206	0.9564	0.8344	0.6250	0.9615	0.6294	0.3176	0.1503	0.5699	0.5870
FCVAE	0.9398	0.7556	0.8624	0.9572	<u>0.8652</u>	0.6995	0.7482	<u>0.8798</u>	0.9650	0.8610	0.6583	0.9653	0.7651	0.3812	0.2857	0.7145	0.6743
LSTMAD	0.9376	0.7742	0.8782	0.9624	0.8633	0.6981	<u>0.7655</u>	0.8740	0.9866	0.9028	0.6743	0.9849	0.7040	0.3482	0.3121	0.6432	0.6808
KAN	0.9411	<u>0.7816</u>	0.8666	0.9664	0.8109	<u>0.6466</u>	<u>0.7518</u>	0.8286	0.9879	<u>0.8939</u>	<u>0.6650</u>	0.9881	0.8016	0.4120	0.3971	0.7489	<u>0.6835</u>
KAN-AD	0.9442	0.7989	<u>0.8755</u>	0.9693	0.9425	0.8940	0.8391	0.9716	0.9888	0.8927	0.6623	<u>0.9868</u>	0.8554	0.5335	0.5177	0.8188	0.7798
	± 0.0007	± 0.0054	± 0.0024	± 0.0008	± 0.0040	± 0.0022	± 0.0055	± 0.0035	± 0.0005	± 0.0025	± 0.0022	± 0.0009	± 0.0040	± 0.0046	± 0.0042	± 0.0041	

Table 4: Efficiency comparison on UCR dataset.

Method	GPU Time	CPU Time	Parameters	$F1_e$
OFA	220s	3087s	81,920 M	0.3176
AT	201s	1152s	4,752 M	0.1696
FCVAE	2327s	1743s	1,414 M	0.3812
TimesNet	182s	259s	73,449	0.1805
LSTMAD	73s	267s	10,421	0.3482
KAN	66s	34s	1,360	0.4120
FITS	32s	17s	624	0.2926
TranAD	113s	62s	369	0.1840
KAN-AD	42s	36s	274	0.5335

4.2.1 Baselines. We conducted comparative experiments with ten state-of-the-art time series anomaly detection methods: LSTMAD [29], FCVAE [40], SRCNN [32], FITS [46], TimesNet [41], OFA [50], TranAD [37], SubLOF [5], Anomaly Transformer [45] (abbreviated as AT in the tables), KAN [27] and SAND [2].

Detailed descriptions of these methods can be found in Appendix B. To ensure the reliability of our experimental results, we directly adopted the hyperparameter settings reported in the original baseline papers for datasets used therein. For datasets not featured in the baseline literature, we meticulously tuned hyperparameters via grid search to optimize the performance of the baseline method on the respective evaluation metrics.

4.2.2 Evaluation metrics. In practical applications, operations teams are less concerned with point-wise anomalies (i.e., whether individual data points are classified as anomalous) and more focused on detecting sustained anomalous segments within time series data. Furthermore, due to the potential impact of such segments, early identification is crucial.

Previous work [44] proposed the **Best F1** metric, which iterates over all thresholds and applies a point adjustment strategy to calculate the F1 score. However, it has been criticized for performance inflation [23, 43]. To address this, we also adopt **Delay F1** [32] and **Event F1**. Delay F1 is similar to Best F1 but uses a delay point adjustment strategy. As shown in Figure 4, the second anomaly was missed because the detection delay exceeded the threshold of five time intervals. In all experiments, a delay threshold of five was used across all datasets. Event F1, on the other hand, treats anomalies of

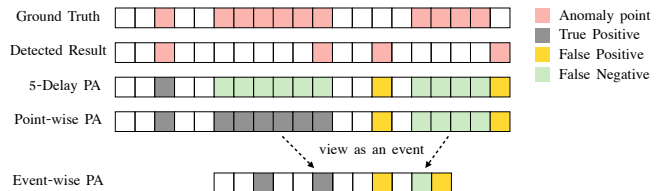


Figure 4: Illustration of the adjustment strategy. Point-wise PA gives an inflated score when some anomaly segments persist for a long duration. Event-wise PA treats each anomaly segment as an event, completely disregarding the length of the anomaly segment. k -delay PA considers only anomalies detected within the first k points after the anomaly onset, treating any detected later as undetected.

varying lengths as anomalies with a length of 1, minimizing performance inflation caused by excessively long anomalous segments. For the sake of convenience, unless otherwise stated, we use Event F1 as the primary metric, as it is more alignment with the need for real-time anomaly detection in real-world situations.

4.3 RQ1. Performance and Efficiency Comparison

We present the results of our time series anomaly detection experiments in Table 3. Table 4 provides inference times for models evaluated on sample from UCR dataset. Notably, our KAN-AD model consistently achieves comparable or superior performance across all experiments.

Despite the absence of anomalies in the UCR dataset’s training set, the presence of significant periodic variations among the samples may reduce the baseline method’s ability to capture normal patterns. For TODS, since its training set includes a substantial number of anomalies, KAN-AD demonstrates a significant advantage over the baseline methods, highlighting the robustness of KAN-AD during the training process. Given the strong periodicity in the WSD and KPI datasets, KAN-AD achieves comparable performance as the baseline methods. Overall, KAN-AD achieves more than a 15% improvement in average Event F1 compared to the state-of-the-art methods.

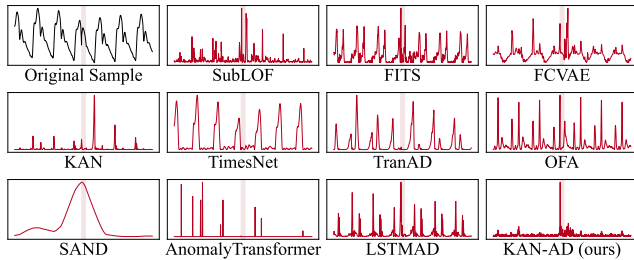


Figure 5: Case study on UCR InternalBleeding10. The black curve represents the original sample, the red curve represents the anomaly scores provided by the method, and the true anomaly segments are highlighted in pink.

As shown in Table 4, some baseline methods are absent compared to those presented in Table 3. This is because methods like SAND can only be executed on CPUs, while traditional approaches such as SubLOF do not leverage multi-core performance. To ensure consistency in our comparisons, we ultimately excluded these methods from the inference time evaluation.

Among the models listed, parameter counts range from millions to hundreds. Notably, large models such as OFA require a staggering number of parameters, reaching 81.92M. Similarly, popular models like Anomaly Transformer, FCAVE, and TimesNet exhibit parameter counts ranging from 73k to 4.75M. In contrast, KAN-AD distinguishes itself as a highly efficient model, achieving impressive performance with only 274 parameters. Significantly, KAN-AD reduces the parameter count by 25% compared to the next smallest model, TranAD.

These analyses highlight the remarkable efficiency of KAN-AD. Despite its small size, KAN-AD consistently achieves competitive results, positioning it as an attractive option for time series anomaly detection tasks. KAN-AD demonstrates that achieving state-of-the-art (SOTA) or near SOTA performance while significantly reducing the parameter footprint is possible, making it an ideal choice for cost-sensitive or resource-constrained environments.

4.3.1 Case Study. We analyzed anomaly detection performance on UCR dataset samples to illustrate how various methods respond to identical anomalies, as shown in Figure 5. The selected sample displayed pattern anomalies, marked by significant deviations from typical behavior.

Both TranAD and TimesNet exhibit difficulty establishing normal temporal patterns. Minor variations among normal samples across cycles lead to periodic false alarms during normal segments, consistent with our observations in Figure 2. Among the methods listed, while OFA, LSTMAD, SubLOF, and FITS can detect anomalies, their high anomaly scores during normal segments indicate excessive sensitivity to minor fluctuations in normal data. In contrast, KAN-AD name excels in identifying anomalies while maintaining minimal anomaly scores during normal segments.

4.4 RQ2. Hyperparameter sensitivity

The KAN-AD model incorporates two key hyperparameters: the number of univariate functions N and the window size T . To investigate the ultimate impact of these parameters on model performance,

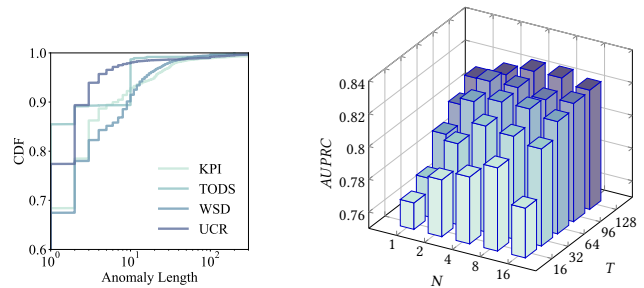


Figure 6: Distribution of anomalous lengths.

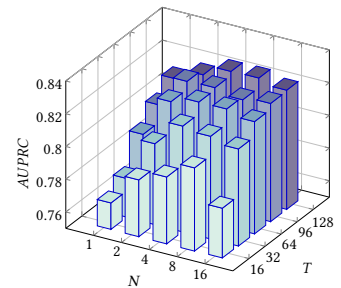


Figure 7: Model performance under different hyperparameters.

we conducted experiments on the UCR dataset while holding all other parameters constant. As findings summarized in Figure 7,

As findings summarized in Figure 7, a larger sliding window facilitates more accurate learning of normal patterns when N is fixed, leading to improved performance. When T is fixed, an optimal number of univariate functions yields the best results. Insufficient univariate functions limit KAN-AD’s expressive power, while excessive N can lead to overfitting.

Overall, KAN-AD achieved its best performance with $T = 96$ and $N = 2$. Notably, even with suboptimal hyperparameter settings like $T = 16$ and $N = 1$, we surpassed SOTA methods on the UCR dataset.

4.5 RQ3. Ablation Studies

To understand the contribution of each module in KAN-AD, we conducted ablation studies. Specifically, we investigated the impact of the differencing module and the influence of different univariate function choices. Additionally, we explored the influence of function deconstruction mechanism on the algorithm’s performance in Appendix C.

4.5.1 Constant term elimination module. We employed a constant term elimination (CTE) module during data preprocessing to mitigate the influence of the offset term A_0 in Equation (3). Further experiments were conducted across all datasets to evaluate the impact of incorporating CTE within the preprocessing pipeline.

As presented in Figure 8, the impact of CTE varies across datasets, reflecting inherent data characteristics. For datasets with pronounced periodicity or strong temporal stability (e.g., WSD), the benefits of CTE are less apparent. Conversely, for datasets exhibiting larger value fluctuations or trends (e.g., KPI, TODS and UCR), CTE yields significant improvements.

4.5.2 Selection of univariate functions. To comprehensively assess the ability of KAN-AD, we conducted experiments using common univariate functions listed in Table 1.

In our implementations, due to varying input range requirements across univariate functions, appropriate normalization techniques are employed. Specifically, min-max scaling to the range $x \in [-1, 1]$ was utilized for both types of Chebyshev polynomials, while z-score was employed for Taylor series and Fourier series. The performance of all four univariate functions was compared using the same configuration.

As results presented in Figure 9, Fourier series consistently achieved the top two performance across all datasets. In contrast,

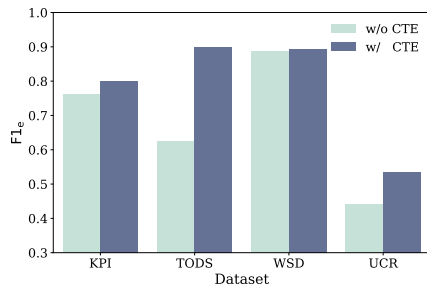


Figure 8: Model performance under different preprocessing.

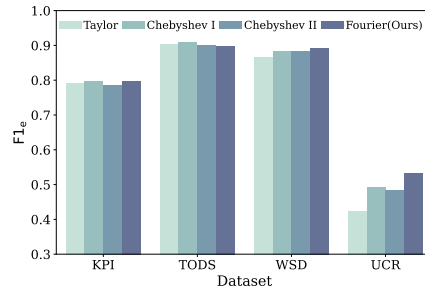


Figure 9: Model performance under different univariate function.

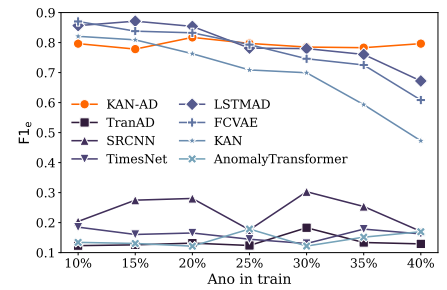


Figure 10: Model performance under different anomaly ratios in training.

Taylor series exhibited persistent bias due to non-zero function values in most cases, hindering optimal model performance. The primary objective of the two types of Chebyshev polynomials is to minimize the maximum error, which conflicts with the Mean Squared Error loss function used by our model. This discrepancy contributed to their suboptimal performance.

4.6 RQ4. Robustness to Anomalous Data

To evaluate KAN-AD’s robustness to anomalies in the training set, we conducted further experiments using the TODS dataset. Specifically, we selected samples with spike anomalies as the test set while progressively increasing the proportion of spike anomalies in the anomaly-free training set. For a fair comparison, we excluded methods that do not involve a training process.

As illustrated in Figure 10, KAN-AD demonstrates stable performance across all anomaly ratios. Popular methods such as LSTMAD, FCVAE, and KAN perform well at lower anomaly ratios but experience a significant decline as the ratio increases. Other approaches, like TimesNet and TranAD, fail to achieve optimal performance due to overfitting to fine-grained structures within the time series.

5 Related Work

Time Series Forecasting Methods :In recent years, methods that use temporal forecasting for establishing normal patterns have dominated the field of time series anomaly detection. These methods evaluate anomalies by calculating the discrepancy between the predicted results and the observed results. An anomaly is considered to occur when this discrepancy exceeds a certain threshold. These methods can be further divided into reconstruction-based and prediction-based approaches.

Reconstruction-based methods, such as Donut [44], assume that normal models exhibit low rank properties and utilize this to denoise time series data. FCVAE [40] further enhance the Variational Autoencoder (VAE) [19] model’s ability to capture normal patterns by incorporating bidirectional dependencies and frequency domain information respectively. With the exploration of Transformer models’ potential, TranAD [37] leverages them as its backbone and employs adversarial learning to capture temporal dependencies within time series. Anomaly Transformer [45] uses the attention mechanism to calculate association discrepancy. OFA [50] further advances the Transformer architecture by incorporating GPT-2 [31] as part of its backbone, enabling it to capture more intricate patterns through a large number of parameters. Similar to the approach of

increasing parameters, TimesNet [41] utilizes a common computer vision (CV) backbone, Inception [36], to transform time series into a two-dimensional representation based on periodicity information for feature modeling.

Prediction-based methods, such as FITS [46] employs low-pass filtering and frequency domain information to model low-frequency components, achieving efficient anomaly detection with minimal parameters. LSTMAD [29], utilize Long Short-Term Memory (LSTM) networks [13] to model normal patterns within time series. By forgetting discrete values, LSTMAD achieves promising detection accuracy.

Pattern Change Detection Methods: Another direct approach to time series anomaly detection focuses on identifying differences between the current time window’s pattern and historical patterns. Statistical approaches like SubLOF [5] quantify pattern differences by calculating distances between sequences in the current window and surrounding windows. Deep learning models such as SRCNN [32] uses supervised training to learn the relationship between anomaly labels and changes in the frequency domain, eventually outputting predicted labels. SAND [2] uses supervised training to learn the relationship between anomaly labels and changes in the frequency domain, eventually outputting predicted labels. Anomaly Transformer [45] constrains the attention mechanism to identify anomalous windows by outputting attention weights. TriAD [35] uses contrastive learning across the time domain, frequency domain, and residual domain to jointly detect pattern changes, achieving state-of-the-art performance on the UCR dataset.

6 Conclusion

Training time series anomaly detection models with datasets containing anomalies is essential for deployment in production environments. Existing algorithms often rely on carefully selected features and complex architectures to achieve minor accuracy gains, neglecting robustness during training. This paper introduces KAN-AD, a robust anomaly detection model rooted in the Kolmogorov–Arnold representation theorem. KAN-AD transforms the prediction of time points into the estimation of coefficients of Fourier series, achieving strong performance with few parameters, significantly reducing costs while enhancing robustness to outliers. Our model includes a constant term elimination module to address temporal trends and leverages frequency domain information for better performance. Compared to the SOTA model across four public datasets, KAN-AD achieves a 15% improvement in average Event F1 score,

while reducing the parameter count by 99% and accelerating inference speed by 55 times.

With KAN-AD, a promising research direction is to explore whether normal patterns in time series can be represented more efficiently by leveraging additional data.

References

- [1] Alexander Dylan Bodner, Antonio Santiago Tepsich, Jack Natan Spolski, and Santiago Pourteau. 2024. Convolutional Kolmogorov–Arnold Networks. arXiv:2406.13155 [cs.CV] <https://arxiv.org/abs/2406.13155>
- [2] Paul Boniol, John Paparrizos, Themis Palpanas, and Michael J Franklin. 2021. SAND: streaming subspace anomaly detection. *Proceedings of the VLDB Endowment* 14, 10 (2021), 1717–1729.
- [3] Ronald Newbold Bracewell and Ronald N Bracewell. 1986. *The Fourier transform and its applications*. Vol. 31999. McGraw-Hill New York.
- [4] Jürgen Braun and Michael Griebel. 2009. On a constructive proof of Kolmogorov’s superposition theorem. *Constructive approximation* 30 (2009), 653–675.
- [5] Markus M Breunig, Hans-Peter Kriegel, Raymond T Ng, and Jörg Sander. 2000. LOF: identifying density-based local outliers. In *Proceedings of the 2000 ACM SIGMOD international conference on Management of data*. 93–104.
- [6] AIOps Competition. 2018. KPI Dataset. <https://github.com/iopsai/iops>.
- [7] C De Boor. 1978. A practical guide to splines. *Springer-Verlag google schola* 2 (1978), 4135–4195.
- [8] Harry Dym and MCKEAN HP. 1972. Fourier series and integrals. (1972).
- [9] Jean Baptiste Joseph Fourier. 1888. *Théorie analytique de la chaleur*. Vol. 1. Gauthier-Villars.
- [10] Siho Han and Simon S. Woo. 2022. Learning Sparse Latent Graph Representations for Anomaly Detection in Multivariate Time Series. In *Proceedings of the 28th ACM SIGKDD Conference on Knowledge Discovery and Data Mining* (Washington DC, USA) (KDD ’22). Association for Computing Machinery, New York, NY, USA, 2977–2986. <https://doi.org/10.1145/3534678.3539117>
- [11] Kaiming He, Xiangyu Zhang, Shaoqing Ren, and Jian Sun. 2016. Deep residual learning for image recognition. In *Proceedings of the IEEE conference on computer vision and pattern recognition*. 770–778.
- [12] Dan Hendrycks and Kevin Gimpel. 2016. Gaussian error linear units (gelus). arXiv preprint arXiv:1606.08415 (2016).
- [13] Sepp Hochreiter and Jürgen Schmidhuber. 1997. Long short-term memory. *Neural computation* 9, 8 (1997), 1735–1780.
- [14] Ruei-Jie Hsieh, Jerry Chou, and Chih-Hsiang Ho. 2019. Unsupervised online anomaly detection on multivariate sensing time series data for smart manufacturing. In *2019 IEEE 12th conference on service-oriented computing and applications (SOCA)*. IEEE, 90–97.
- [15] Alexis Huet, Jose Manuel Navarro, and Dario Rossi. 2022. Local Evaluation of Time Series Anomaly Detection Algorithms. In *Proceedings of the 28th ACM SIGKDD Conference on Knowledge Discovery and Data Mining* (Washington DC, USA) (KDD ’22). Association for Computing Machinery, New York, NY, USA, 635–645. <https://doi.org/10.1145/3534678.3539339>
- [16] Kyle Hundman, Valentino Constantinou, Christopher Laporte, Ian Colwell, and Tom Soderstrom. 2018. Detecting spacecraft anomalies using lstms and nonparametric dynamic thresholding. In *Proceedings of the 24th ACM SIGKDD international conference on knowledge discovery & data mining*. 387–395.
- [17] Sergey Ioffe and Christian Szegedy. 2015. Batch normalization: Accelerating deep network training by reducing internal covariate shift. In *International conference on machine learning*. pmlr, 448–456.
- [18] Tung Kieu, Bin Yang, Chenjuan Guo, Razvan-Gabriel Cirstea, Yan Zhao, Yale Song, and Christian S Jensen. 2022. Anomaly detection in time series with robust variational quasi-recurrent autoencoders. In *2022 IEEE 38th International Conference on Data Engineering (ICDE)*. IEEE, 1342–1354.
- [19] Diederik P Kingma and Max Welling. 2022. Auto-Encoding Variational Bayes. arXiv:1312.6114 [stat.ML]
- [20] Andrei Nikolaevich Kolmogorov. 1957. On the representation of continuous functions of many variables by superposition of continuous functions of one variable and addition. In *Doklady Akademii Nauk*, Vol. 114. Russian Academy of Sciences, 953–956.
- [21] Andrei Nikolaevich Kolmogorov. 1961. *On the representation of continuous functions of several variables by superpositions of continuous functions of a smaller number of variables*. American Mathematical Society.
- [22] Kwei-Herng Lai, Daochen Zha, Junjie Xu, Yue Zhao, Guanchu Wang, and Xia Hu. 2021. Revisiting time series outlier detection: Definitions and benchmarks. In *Thirty-fifth conference on neural information processing systems datasets and benchmarks track (round 1)*.
- [23] Kwei-Herng Lai, Daochen Zha, Junjie Xu, Yue Zhao, Guanchu Wang, and Xia Hu. 2021. Revisiting time series outlier detection: Definitions and benchmarks. In *Thirty-fifth conference on neural information processing systems datasets and benchmarks track (round 1)*.
- [24] Dan Li, Dacheng Chen, Baihong Jin, Lei Shi, Jonathan Goh, and See-Kiong Ng. 2019. MAD-GAN: Multivariate anomaly detection for time series data with generative adversarial networks. In *International conference on artificial neural networks*. Springer, 703–716.
- [25] Zhihan Li, Youjian Zhao, Jiaqi Han, Ya Su, Rui Jiao, Xidao Wen, and Dan Pei. 2021. Multivariate time series anomaly detection and interpretation using hierarchical inter-metric and temporal embedding. In *Proceedings of the 27th ACM SIGKDD conference on knowledge discovery & data mining*. 3220–3230.
- [26] Ziming Liu, Pingchuan Ma, Yixuan Wang, Wojciech Matusik, and Max Tegmark. 2024. KAN 2.0: Kolmogorov–Arnold Networks Meet Science. arXiv:2408.10205 [cs.LG] <https://arxiv.org/abs/2408.10205>
- [27] Ziming Liu, Yixuan Wang, Sachin Vaidya, Fabian Ruehle, James Halverson, Marin Soljačić, Thomas Y Hou, and Max Tegmark. 2024. Kan: Kolmogorov–arnold networks. arXiv preprint arXiv:2404.19756 (2024).
- [28] Pankaj Malhotra, Anusha Ramakrishnan, Gaurangi Anand, Lovekesh Vig, Puneet Agarwal, and Gautam Shroff. 2016. LSTM-based encoder-decoder for multi-sensor anomaly detection. arXiv preprint arXiv:1607.00148 (2016).
- [29] Pankaj Malhotra, Lovekesh Vig, Gautam Shroff, Puneet Agarwal, et al. 2015. Long Short Term Memory Networks for Anomaly Detection in Time Series.. In *Esann*, Vol. 2015. 89.
- [30] Xinji Qu, Zhuo Liu, Chase Q Wu, Aiqin Hou, Xiaoyan Yin, and Zhulian Chen. 2024. MFGAN: Multimodal Fusion for Industrial Anomaly Detection Using Attention-Based Autoencoder and Generative Adversarial Network. *Sensors* 24, 2 (2024), 637.
- [31] Alec Radford, Jeffrey Wu, Rewon Child, David Luan, Dario Amodei, Ilya Sutskever, et al. 2019. Language models are unsupervised multitask learners. *OpenAI blog* 1, 8 (2019), 9.
- [32] Hansheng Ren, Bixiong Xu, Yujing Wang, Chao Yi, Congrui Huang, Xiaoyu Kou, Tony Xing, Mao Yang, Jie Tong, and Qi Zhang. 2019. Time-series anomaly detection service at microsoft. In *Proceedings of the 25th ACM SIGKDD international conference on knowledge discovery & data mining*. 3009–3017.
- [33] Bernhard Schölkopf, Robert C Williamson, Alex Smola, John Shawe-Taylor, and John Platt. 1999. Support vector method for novelty detection. *Advances in neural information processing systems* 12 (1999).
- [34] Elias M Stein and Rami Shakarchi. 2011. *Fourier analysis: an introduction*. Vol. 1. Princeton University Press.
- [35] Yuting Sun, Guansong Pang, Guanhua Ye, Tong Chen, Xia Hu, and Hongzhi Yin. 2024. Unraveling theAnomaly in Time Series Anomaly Detection: A Self-supervised Tri-domain Solution. In *2024 IEEE 40th International Conference on Data Engineering (ICDE)*. IEEE.
- [36] Christian Szegedy, Wei Liu, Yangqing Jia, Pierre Sermanet, Scott Reed, Dragomir Anguelov, Dumitru Erhan, Vincent Vanhoucke, and Andrew Rabinovich. 2015. Going deeper with convolutions. In *Proceedings of the IEEE conference on computer vision and pattern recognition*. 1–9.
- [37] Shreshth Tuli, Giuliano Casale, and Nicholas R Jennings. 2022. TranAD: deep transformer networks for anomaly detection in multivariate time series data. *Proceedings of the VLDB Endowment* 15, 6 (2022), 1201–1214.
- [38] Xing Wang, Jessica Lin, Nital Patel, and Martin Braun. 2016. A self-learning and online algorithm for time series anomaly detection, with application in CPU manufacturing. In *Proceedings of the 25th ACM International Conference on Information and Knowledge Management*. 1823–1832.
- [39] Yue Wang, Michael Perry, Dane Whitlock, and John W Sutherland. 2022. Detecting anomalies in time series data from a manufacturing system using recurrent neural networks. *Journal of Manufacturing Systems* 62 (2022), 823–834.
- [40] Zexin Wang, Changhua Pei, Minghua Ma, Xin Wang, Zhihan Li, Dan Pei, Saravan Rajmohan, Dongmei Zhang, Qingwei Lin, Haiming Zhang, Jianhui Li, and Gaogang Xie. 2024. Revisiting VAE for Unsupervised Time Series Anomaly Detection: A Frequency Perspective. In *Proceedings of the ACM on Web Conference 2024* (<conf-loc>, <city>Singapore</city>, <country>Singapore</country>, </conf-loc>) (WWW ’24). Association for Computing Machinery, New York, NY, USA, 3096–3105. <https://doi.org/10.1145/3589334.3645710>
- [41] Haixu Wu, Tengge Hu, Yong Liu, Hang Zhou, Jianmin Wang, and Mingsheng Long. 2023. TimesNet: Temporal 2D-Variation Modeling for General Time Series Analysis. In *International Conference on Learning Representations*.
- [42] Renjie Wu and Eamonn J Keogh. 2021. Current time series anomaly detection benchmarks are flawed and are creating the illusion of progress. *IEEE transactions on knowledge and data engineering* 35, 3 (2021), 2421–2429.
- [43] Renjie Wu and Eamonn J Keogh. 2021. Current time series anomaly detection benchmarks are flawed and are creating the illusion of progress. *IEEE transactions on knowledge and data engineering* 35, 3 (2021), 2421–2429.
- [44] Haowen Xu, Wenxiao Chen, Nengwen Zhao, Zeyan Li, Jiahao Bu, Zhihan Li, Ying Liu, Youjian Zhao, Dan Pei, Yang Feng, et al. 2018. Unsupervised anomaly detection via variational auto-encoder for seasonal kpis in web applications. In *Proceedings of the 2018 world wide web conference*. 187–196.
- [45] Jiehui Xu, Haixu Wu, Jianmin Wang, and Mingsheng Long. 2022. Anomaly Transformer: Time Series Anomaly Detection with Association Discrepancy. In *International Conference on Learning Representations*. https://openreview.net/forum?id=LzQQ89U1qm_

- [46] Zhijian Xu, Ailing Zeng, and Qiang Xu. 2024. FITS: Modeling Time Series with 10k Parameters. In *International Conference on Learning Representations (ICLR)*.
- [47] Runpeng Yu, Weihao Yu, and Xinchao Wang. 2024. Kan or mlp: A fairer comparison. *arXiv preprint arXiv:2407.16674* (2024).
- [48] Peng Zhan, Shaokun Wang, Jun Wang, Leigang Qu, Kun Wang, Yupeng Hu, and Xueqing Li. 2021. Temporal anomaly detection on IIoT-enabled manufacturing. *Journal of Intelligent Manufacturing* 32 (2021), 1669–1678.
- [49] Shenglin Zhang, Zhenyu Zhong, Dongwen Li, Qiliang Fan, Yongqian Sun, Man Zhu, Yuzhi Zhang, Dan Pei, Jiyun Sun, Yinlong Liu, et al. 2022. Efficient kpi anomaly detection through transfer learning for large-scale web services. *IEEE Journal on Selected Areas in Communications* 40, 8 (2022), 2440–2455.
- [50] Tian Zhou, Peisong Niu, Liang Sun, Rong Jin, et al. 2023. One fits all: Power general time series analysis by pretrained lm. *Advances in neural information processing systems* 36 (2023), 43322–43355.

A Datasets

We selected four datasets from diverse domains, with samples originating from:

- **KPI** [6]: This dataset comprises service metrics collected from five major Internet companies: Sogou, eBay, Baidu, Tencent, and Alibaba. The data points are primarily recorded every 1-2 minutes, with some sections exhibiting a 5-minute interval.
- **TODS** [22]: TODS comprises artificially created time series, each designed to present specific types of anomalies. Its excellent interpretability and carefully constructed data distributions make it suitable for in-depth case studies.
- **WSD** [49]: This dataset consists of web server metrics collected from three companies providing large-scale web services: Baidu, Sogou, and eBay.
- **UCR** [42]: This archive contains data from multiple domains with a single anomalous segment on each time series. In addition to real anomalies, UCR also includes synthetic but highly plausible anomalies.

B Baselines

We selected the following baseline approaches to further elaborate on the performance differences between KAN-AD and SOTA methods:

- **SubLOF** [5] represents traditional outlier detection techniques based on distance metrics.
- **SRCNN** [32] is a supervised approach reliant on high-quality labeled data.
- **LSTMAD** [29] leverages Long Short-Term Memory (LSTM) networks [13] for deep learning-based anomaly detection.
- **FITS** [46] achieves parameter-efficient anomaly detection by upsampling frequency domain information using a low-pass filter and simple linear layers.
- **FCVAE** [40] is unsupervised reconstruction method based on Variational Autoencoder (VAE) [19], designed to reconstruct normal patterns.
- **Anomaly Transformer** [45] employs attention mechanism to compute the association discrepancy.
- **TranAD** [37] incorporates the principles of adversarial learning to develop a training framework with two stages while integrating the strengths of self-attention encoders to capture the temporal dependency embedded in the time series.

Table 5: Model performance under different function deconstruction strategies.

Variation	F1 _e	F1 _d	AUPRC
KAN-AD	0.5335	0.5177	0.8188
w/o X	0.5153	0.4974	0.8066
w/o P	0.5081	0.4810	0.8007
w/o S	0.5056	0.5113	0.7998
w/o X&P	0.4737	0.4583	0.7872
w/o X&S	0.4698	0.4610	0.7767
w/o S&P	0.4561	0.4637	0.7595

- **SAND** [2] utilizes a novel statistical approach based on curve shape clustering for anomaly detection in a streaming fashion.
- **TimesNet** [41] leverages an Inception [36]-based computer vision backbone to enhance learning capabilities.
- **OFA** [50], with GPT-2 [31] as its backbone, improves its ability to capture point-to-point dependencies.
- **KAN** [27] leverages Kolmogorov-Arnold representation theory to decompose complex learning objectives into linear combinations of univariate functions.

These baseline methods encompass a variety of anomaly detection paradigms: shape-based SAND, subsequence distance-based SubLOF, Transformer-based approaches like OFA, TranAD, and Anomaly Transformer for modeling sequence relationships, and frequency domain information enhanced methods FCVAE and FITS.

C Ablation on function deconstruction mechanism

To investigate the impact of the FD mechanism, we compared the model’s detection capabilities under different univariate function combination strategies. For clarity, the specific definitions are provided in Equation (7).

As the results presented in Table 5, the model’s detection performance exhibited a notable improvement with an increasing number of univariate functions. Both Fourier series and cosine waves outperformed the raw input data, likely due to their smoother representations compared to the original signal, enabling higher detection accuracy. The combination of different features, particularly those involving Fourier series and cosine waves, resulted in significant performance gains as the feature count increased. Ultimately, KAN-AD achieved optimal detection performance by integrating all features. It is worth noting that even the variant of KAN-AD utilizing only the raw time series X outperforms KAN, clearly demonstrating the advantage of Fourier series over the use of spline functions for optimizing univariate functions.